Geophysical Research Letters

RESEARCH LETTER
10.1029/2018GL081219

Kinetic Simulations of Electron Acceleration by Dispersive Scale Alfvén Waves in Jupiter's Magnetosphere

P. A. Damiano[1], P. A. Delamere[1], B. Stauffer[1], C.-S. Ng[1], and J. R. Johnson[2]

[1]Geophysical Institute, University of Alaska Fairbanks, Fairbanks, AK, USA, [2]Department of Engineering and Computer Science, Andrews University, Berrien Springs, MI, USA

Key Points:
- The first full flux tube kinetic simulations of electron energization in dispersive Alfven waves at Jupiter are presented
- The resulting electron energization is broadband in nature—consistent with recent Juno observations
- The ratio of the torus to high-latitude density plays an important role in regulating the magnitude of the energization

Correspondence to:
P. A. Damiano,
padamiano@alaska.edu

Citation:
Damiano, P. A., Delamere, P. A., Stauffer, B., Ng, C.-S., & Johnson, J. R. (2019). Kinetic simulations of electron acceleration by dispersive scale Alfvén waves in Jupiter's magnetosphere. *Geophysical Research Letters*, *46*, 3043–3051. https://doi.org/10.1029/2018GL081219

Received 12 NOV 2018
Accepted 25 FEB 2019
Accepted article online 4 MAR 2019
Published online 22 MAR 2019

Abstract Electron acceleration by dispersive scale Alfvén waves at Jupiter is investigated using a Gyrofluid-Kinetic-Electron model. Specifically, the simulations consider the propagation of an Alfvén wave perturbation from the center of the Io plasma torus to high-latitude regions that are consistent with recent Juno satellite observations (e.g., Allegrini et al., 2017, https://doi.org/10.1002/2017GL073180; Mauk, et al., 2017a, https://doi.org/10.1038/nature23648; Mauk, et al., 2017b, https://doi.org/10.1002/2016GL072286; Szalay et al., 2018, https://doi.org/10.1029/2018JE005752). As in those observations, the energized electron spectra is broadband in nature and the majority of the energization is under the interaction of inertial Alfvén waves at high latitudes. The extent of the energization associated with these waves is proportional to both the magnitude of the wave perturbation and the ratio of the torus to high-latitude density.

Plain Language Summary Recent observations of the Juno satellite at Jupiter illustrate that the electron energy spectrum at high latitudes is observed to be broadband—that is, ranging in energies from tens of electron volts to tens and hundreds of kiloelectron volts. At Earth, such electron spectra are associated with electron energization by Alfvén waves—which are transverse waves that travel along magnetic field lines in close analogy to waves on a string. In particular, at small scales (e.g., perpendicular scale lengths on the order of the ion orbit around the field line), kinetic effects allow for significant electric field generation that can efficiently accelerate electrons parallel to the field line. At these scales, the waves are known as dispersive Alfvén waves. In this work, we, for the first time, present global-scale (entire dipolar field line) kinetic simulations of electron energization at Jupiter. We illustrate that these dispersive Alfvén waves, sourced in the Io plasma torus, lead to broadband electron energization close to the Jupiter ionosphere that is qualitatively consistent with the Juno observations. We additionally illustrate how the presence of the Io plasma torus (which is a feature unique to the Jupiter ionosphere) affects the characteristics of this broadband energization.

1. Introduction

It has been the traditional view that the auroral acceleration at Jupiter was expected to be largely monoenergetic in nature (associated with the formation of quasi-static potential drops; e.g., Cowley & Bunce, 2001; Ray et al., 2010). However, the recent observations (Allegrini et al., 2017; Mauk, et al., 2017a, 2017b; Szalay et al., 2018) of the Jovian Auroral Distributions Experiment (McComas et al., 2017) and Jupiter Energetic Particle Detector Instrument (e.g., Mauk, Haggerty, Jaskulek, et al., 2017) instruments on the Juno spacecraft have illustrated a largely broadband energization, more consistent with terrestrial Alfvénic aurora. This broadband energization is evident in the main and polar aurora (Allegrini et al., 2017; Mauk et al., 2017a, 2017b) as well as the satellite footprints and tails (Szalay et al., 2018) and in the terrestrial context is commonly associated with electron energization in dispersive scale Alfvén waves (e.g., Chaston, Bonnell, Carlson, McFadden, Ergun, & Strangeway, 2003; Chaston et al., 2002; Keiling et al., 2003; Wing et al., 2013). These waves are Alfvén waves that have perpendicular scale lengths on the order of the ion gyroradius (ρ_i), ion acoustic length (ρ_s), or the electron inertial scale length (e.g., Lysak & Lotko, 1996). In the plasma torus, waves are in the kinetic Alfvén regime (where ρ_s and ρ_i are the defining scale lengths), while at high latitudes, electron inertial (λ_e) effects dominate.

While dispersive scale Alfvén waves have not been directly observed at Jupiter, Alfvénic acceleration has long been invoked for Io's auroral footprint and the associated wake (e.g., Bonfond et al., 2017; Chust et al., 2005; Crary, 1997; Hess et al., 2010; Su et al., 2006; Szalay et al., 2018) and it is suggestive that Chust et al. (2005) noted small-scale magnetic field fluctuations near Io. Theoretical studies have predicted that $E_{||}$ in inertial Alfvén waves would lead to generation of electron beams (e.g., Crary, 1997; Saur et al., 2018). Su et al. (2006) also considered the propagation of dispersive scale Alfvén waves in the Io-Jupiter interaction using a gyrofluid model, but without coupling to kinetic electrons. Motivated by the Chust et al. (2005) observations, Hess et al. (2010) illustrated that a power law distribution provided the optimal scenario to transmit the necessary power to explain auroral emissions. They also found that electron energization at kinetic scales resulted in Kappa type distributions. More recently, Bonfond et al. (2017), using Monte Carlo simulations, illustrated that the vertical brightness profiles evident in the Io footprint tail were best explained by broadband acceleration from Alfvénic processes rather than electron acceleration in quasi-static parallel potential drops.

Power law energy distributions are commonly associated with turbulent cascades, and turbulent processes are believed to dominate in the Jupiter magnetodisc. Both Saur (2004) and Ng et al. (2018) postulated turbulent heating models of the magnetodisc (based on flux tube diffusion and advection respectively), which reproduced characteristics of the observed ion temperature gradient within Jupiter's magnetodisc. Additionally, recent hybrid simulations of Kelvin-Helmholtz (Delamere et al., 2018) and Rayleigh-Taylor (Stauffer, 2018) instabilities, which are common in the magnetodisc, illustrate a turbulent cascade of energy to kinetic scale lengths. In all these cases, the turbulent cascade is aided by the nonlinear interaction of counter-propagating Alfvén waves (Iroshnikov, 1963; Kraichnan, 1965; Ng & Bhattacharjee, 1996; Saur et al., 2002) within the torus. The resulting deposition of Alfvénic energy at kinetic scale lengths can then facilitate the energization of both electrons and ions (Johnson & Cheng, 2001) by dispersive scale Alfvén waves.

In the present work, we do not consider the cross-scale coupling of wave energy but assume the existence of small-scale Alfvén perturbations in the Io plasma torus and for the first time (in kinetic simulation) self-consistently follow the evolution of the interaction between the Alfvén waves and electrons from this source region to the high latitudes. For this investigation we use the Gyrofluid-Kinetic-Electron (GKE) model (Damiano et al., 2015), which has also been used for the study of electron energization in both large-scale (Damiano & Wright, 2008; Damiano & Johnson, 2012) and dispersive scale (Damiano et al., 2015; 2016; Damiano et al., 2018) Alfvén waves in the terrestrial magnetosphere. The remainder of the paper is divided into three sections. Section 2 outlines the GKE model. Section 3 presents the model simulation results, while section 4 gives our conclusions.

2. GKE Model

The simulations were performed with an extension of the hybrid 2-D GKE model (described in Damiano et al., 2015) including a correction (e.g., Gombosi et al., 2002; Hess et al., 2010), which is sometimes termed semirelativistic, so that the wave speed does not exceed the speed of light due to the effects of the displacement current. Using the Jupiter magnetic dipole moment $M_J = 1.55 \times 10^{27}$ Am^2, the ambient dipolar model geometry considered in the simulations is illustrated in Figure 1a where x_1 and x_2 are the field-aligned and radial directions, respectively. There is no dependence on the azimuthal coordinate so that $\partial/\partial x_3 = 0$.

The gyrofluid portion of the model incorporates the modified linearized momentum equation given by

$$\mu_o \rho_o \frac{\partial \tilde{u}_3}{\partial t} = \gamma_A^2 \frac{B_o}{h_1 h_3} \left(\frac{\partial}{\partial x_1} \left(h_3 b_3 \right) \right) \tag{1}$$

where u_3 and b_3 are respectively the azimuthal fluid velocity and magnetic field perturbations, $\gamma^{-2} = 1 + V_A^2/c^2$, $\tilde{u}_3 = (1 - 1.25\rho_i^2 \nabla_\perp^2) u_3$, $\rho_i = (T_i/m_i)^{1/2}/\Omega_i$ is the ion gyroradius, $x_1 = \cos\theta/r^2$, $x_2 = \sin^2\theta/r$, $x_3 = \phi$, $h_1 = r^3/(1 + 3\cos^2\theta)^{1/2}$, $h_2 = r^2/(\sin\theta(1 + 3\cos^2\theta)^{1/2})$, $h_3 = r\sin\theta$, and B_o and ρ_o denote respectively the background magnetic field and plasma density, while T_i is the ion temperature, m_i is the ion mass, and Ω_i is the ion gyrofrequency. The corresponding nonrelativistic Alfvén speed is then given by $V_A = B_o/\sqrt{\mu_o \rho_o}$. Equation (1) is coupled to Faraday's law

$$\frac{\partial b_3}{\partial t} = \frac{-1}{h_1 h_2} \left(\frac{\partial}{\partial x_1} \left(h_2 E_2 \right) - \frac{\partial}{\partial x_2} \left(h_1 E_1 \right) \right) \tag{2}$$

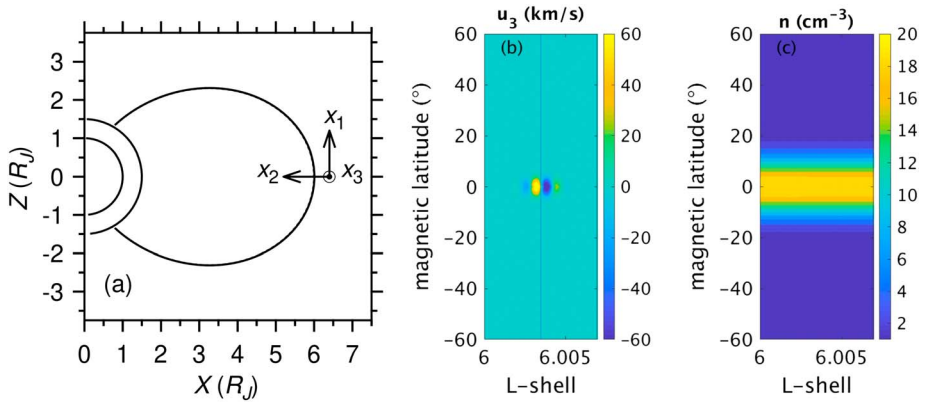

Figure 1. (a) Simulation domain centered on $L = 6.0035$ field line. The flux tube is too narrow to differentiate radial boundaries on this scale (set at $L = 6.0$ and $L = 6.007$, respectively). The circles of radius 1 and 1.5 R_J, respectively, denote the surface of Jupiter and the model low-altitude boundary. (b) Initial azimuthal velocity perturbation as a function of L shell and magnetic latitude. (c) Simulation density profile where the peak centered on 0° magnetic latitude is indicative of the plasma torus.

and the Generalized Ohm's law gives the perpendicular

$$E_2 = -B_o(1 - \rho_i^2 \nabla_\perp^2)\tilde{u}_3 \tag{3}$$

and parallel electric fields

$$E_{||} = \mu_o \lambda_e^2 \frac{\partial j_{||}}{\partial t} - \frac{1}{ne}\nabla_{||} P_{e_{||}} - \frac{1}{ne}\frac{P_{e_{||}} - P_{e_\perp}}{B_o}\nabla_{||} B_o \tag{4}$$

where $\lambda_e = \sqrt{m_e/\mu_o n e^2}$ is the electron inertial length and this equation is displayed in conventional form for simplicity. The full form (and derivation) is presented in Damiano et al. (2007).

The parallel electron dynamics are described using the guiding center equations

$$m_e \frac{dv_1}{dt} = -eE_1 - \mu_m \frac{1}{h_1}\frac{\partial B_o}{\partial x_1} \tag{5}$$

$$h_1 \frac{dx_1}{dt} = v_1 \tag{6}$$

where $v_1 = v_{||}$ is the parallel electron velocity, $\mu_m = m_e v_\perp^2/(2B)$ is the magnetic moment, and $v_\perp$ is the gyrophase independent perpendicular velocity ($v_\perp = \sqrt{v_2^2 + v_3^2}$). The integral moments of the electron distribution function for use in the parallel Ohm's law are determined using standard Particle-In-Cell techniques (Damiano et al., 2007). The semirelativistic correction has been applied to the momentum equation because, relative to the terrestrial magnetosphere, the densities are so low, and the magnetic fields so high in the magnetospheres of the giant planets, that the Alfvén speed can approach the speed of light.

At the low-altitude boundaries, perfectly conducting boundary conditions are imposed, while a node in parallel current ($j_{||} = 0$) is assumed at the perpendicular boundaries (Damiano & Johnson, 2012; Damiano et al., 2007). For the present simulations, the low-altitude boundary has been set at the altitude of 1.5 R_J. This height is approximately consistent with the height below which the density is thought to increase dramatically toward the Jupiter ionosphere (e.g., parallel density profile considered in Su et al., 2006) and consequently the position of the B/n peak. Below this peak, electron energization is expected to be limited since in the dramatic increase in electron density means less acceleration is required to carry the parallel current (e.g., Wright et al., 2002, in the terrestrial context).

3. Simulations

The simulations are initialized by the azimuthal velocity perturbation displayed in Figure 1b, while the initial density profile is displayed in Figure 1c. The density peak in the middle of the simulation domain

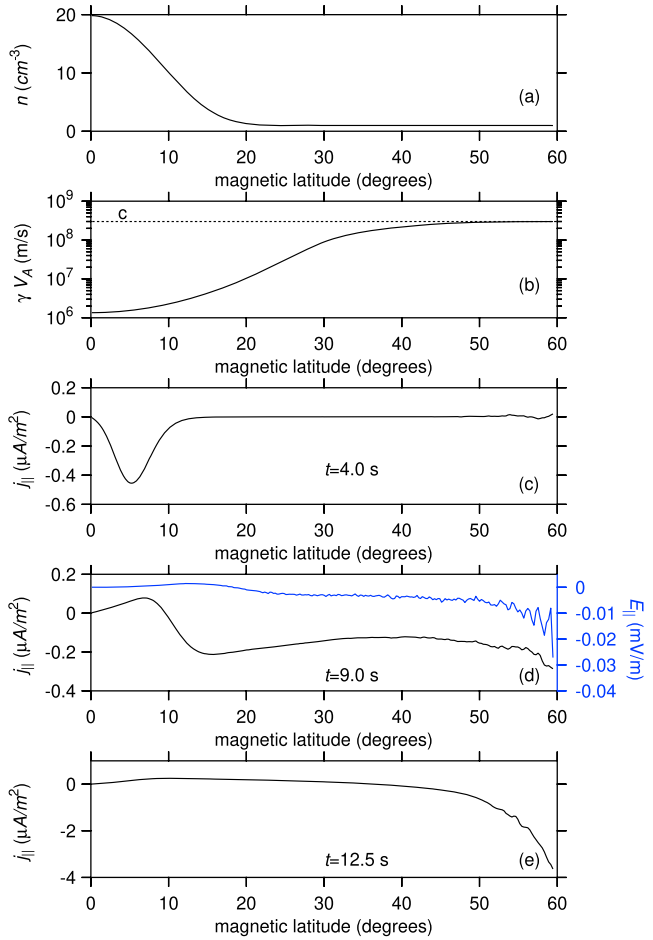

Figure 2. (a) Initial density profile as a function of magnetic latitude. (b) Corresponding relativistic Alfvén speed profile. (c—e) Profile of parallel current at indicated times. Panel (d) also illustrates the corresponding parallel electric field. Small-scale fluctuations apparent at large magnetic latitudes ($\gtrsim$50°) are due to statistical noise near the low-altitude boundary where the number of simulation particles per grid cell is less than in the equatorial region. All profiles are taken along the central $L = 6.0035$ field line.

is meant to approximate the presence of the Io plasma torus. For simplicity in this initial investigation, we limit the peak torus density to be a factor of 20 (Figure 2a) over the high-latitude density (set at a value of 1 cm^{-3}). We additionally assume that the torus is composed exclusively of hydrogen in order to increase the magnitude of the Alfvén speed profile within the torus which allows the wave perturbation to propagate out of the torus in a more computationally reasonable amount of time. The perpendicular scale length of the perturbation (Figure 1b) in the equatorial plane maps to the order of electron inertial scale lengths at high latitudes (which for the given density profile yields $\lambda_e = 5.3$ km and is close to the peak value considered in the study of Su et al., 2006).

Figure 2 displays the evolution of the parallel current profile along the central field line of the simulation domain (indicated by the vertical line in Figure 1a—which is also the field line of maximum $j_{||}$). The original velocity perturbation was chosen to have a peak amplitude of 100 km/s, which is order of magnitude consistent with either the relative velocity between Io and the torus (57 km/s) or observed injection flows (e.g., Thorne et al., 1997). This initial perturbation splits up into two identical perturbations that propagate toward the opposing low-altitude boundaries. Since the pulse profiles are symmetric, we plot only the current profiles at different times for the northern simulation hemisphere as a function of magnetic latitude (Figures 2c–2e). As the pulse propagates through the torus boundary, part of the energy is transmitted and part is reflected (Figure 2c). The profile of the transmitted wave signature becomes extended along the field line owing to the dramatic increase in the Alfvén speed (which reaches the speed of light close to the low-altitude boundary). The moment of peak parallel current at the low-altitude boundary is plotted in

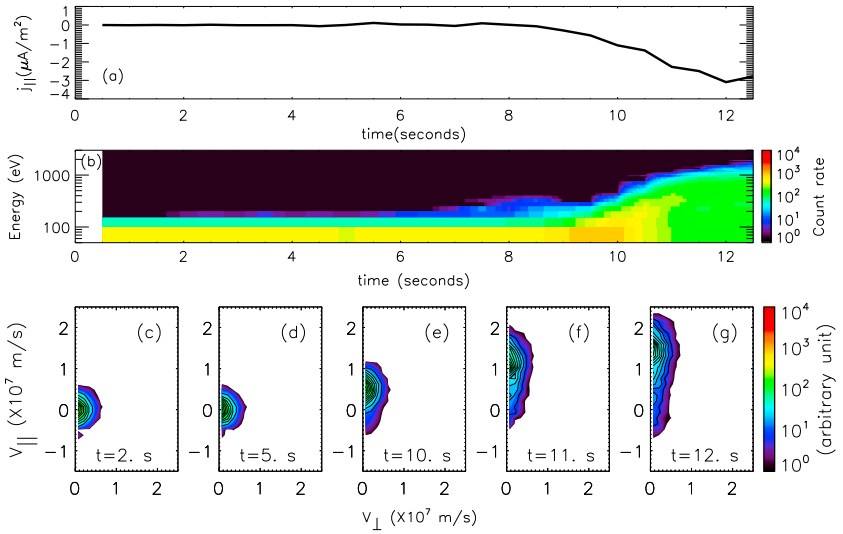

Figure 3. (a) Parallel current above the low-altitude boundary as a function of time. (b) Electron energy spectrogram above the northern low-altitude boundary in arbitrary unit. To construct the spectrogram, simulation electrons were binned in 50-eV energy intervals. (c–g) Electron distribution functions at the indicated times. Initial electron temperature (T_e) considered in all simulations is 20 eV.

Figure 2e where the dramatic increase in the magnitude of $j_{||}$ is due to the converging magnetic field topology. Figure 2d also illustrates the corresponding parallel electric field profile (which has been spatially and temporally averaged [over a 0.5-s interval] to reduce the amount of statistical noise). As would be expected, the profile of the parallel electric field increases in magnitude consistent with the parallel current as the low-altitude boundary is approached. The slight positive peak in $E_{||}$ at about 13° magnetic latitude is associated with the density gradient and reflection of wave energy in the gradient. This field is a superposition of the ambipolar electric field that maintains the density gradient and the wave-parallel electric field. A more complete examination of the evolution of the parallel electric field will be considered in a subsequent study, but the evolution of the parallel electric field for a standing wave in an Alfvén speed gradient is presented in Damiano et al. (2005).

In order to directly compare the parallel current and electron signatures, $j_{||}$ as a function of time at the northern ionospheric boundary is plotted in Figure 3a along with a spectrogram of the electron energy above this boundary (Figure 3b), which is constructed by stacking histograms of the electron count versus energy at specific times (e.g., Figures 4b and 5b). The corresponding distribution functions at select times are plotted in Figures 3c–3g. Comparison of Figures 3a and 3b illustrates that the peak of the parallel current coincides with the maximum range of electron energies that are broadband in nature, in qualitative agreement with the aforementioned Juno observations (e.g., Allegrini et al., 2017; Mauk, et al., 2017a, 2017b). The negative parallel current is being carried by a positive displacement of the electron distribution function ($j_e = -nev_{||}$) that becomes highly field-aligned as the current peaks (Figures 3c–3g). Both the broadband energization and field-aligned distributions are also in agreement with signatures of Alfvénic aurora evident at Earth (e.g., Chaston, Bonnell, Carlson, McFadden, Ergun, & Strangeway, 2003). The fact that the electron energization peaks with the parallel current implies that the primary electron energization is happening in the inertial Alfvén wave regime just above the low-altitude boundary. Kletzing (1994) noted that electron energization in the inertial Alfvén wave limit involves both nonresonant and resonant (Fermi) components (where Fermi-type electron acceleration at Io was also specifically discussed by Crary, 1997). The nonresonant acceleration involves the energization of the bulk electron distribution to carry the parallel current. As the parallel current and the electron acceleration are peaking coincidentally in Figure 3, it is clear that in this case the energization is mainly associated with the nonresonant interaction and that resonant Fermi-type energization (the evidence of which should be preceding the current signature) is not playing a significant role for the parameters selected here. For the Fermi acceleration to happen, the resonant electron kinetic energy (in the wave frame), must be less than the wave potential drop (Kletzing, 1994). For a given electron distribution temperature, this resonance condition is more difficult to achieve as wave speed increases and so it is possible that this type of energization might be less prevalent at Jupiter (where the wave phase speed

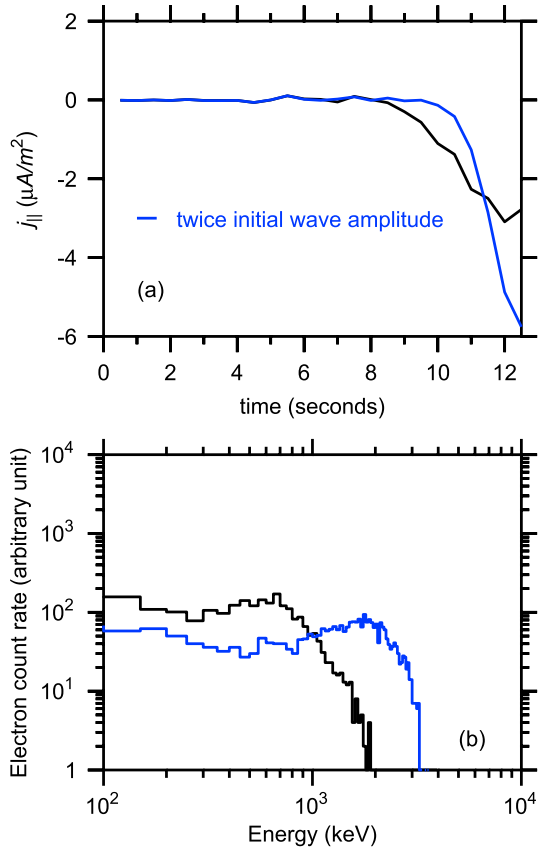

Figure 4. (a) Parallel current above the low-altitude boundary as a function of time for original (from Figure 3a) and case with twice initial wave amplitude (blue line). Latter simulation was initialized by doubling the magnitude of the shear velocity perturbation given in Figure 1b, which also doubles the amplitude of the wave magnetic field. (b) Corresponding histograms of electron count rate versus energy above low-altitude boundary at $t = 12.5$ s.

reaches the speed of light) than at Earth. However, a more careful consideration of the nature of the electron energization for a wider parameter range will be the focus of a future study.

The bulk energization that carries the parallel current should be proportional to the magnitude of the current and hence the magnitude of the wave amplitude. This point is confirmed in Figure 4, which compares the parallel current at the low-altitude boundary (Figure 4a) and the corresponding histograms of electron energy (Figure 4b). Both the resulting current and energization are larger in the case with twice initial wave amplitude.

One of the fundamental differences between the terrestrial and Jovian systems is the presence of the Io plasma torus. In order to understand what role the presence of the torus can play in the characteristics of the Alfvénic aurora, we conducted a simulation lacking an equatorial density torus, but with the same initial shear (u_3) velocity perturbation considered in Figure 3. The results are plotted in Figure 5 where the parallel current signature peaks much sooner in the no torus case (Figure 5a) because the Alfvén speed is inversely proportional to the density. Interestingly, both the magnitude of the parallel current and electron energization are significantly larger in the torus case in spite of the fact that the initial velocity profiles are identical in both cases. This increase, at first glance, seems counter to what is expected given the results of Figure 4. However, even though the initial velocity is the same in both cases, the increased density of the torus implies a reduced wave group velocity (and increased ion kinetic energy), which, by the Walen relation, results in an increased amplitude for the wave magnetic field (and thus increased Poynting flux). The larger magnetic field perturbation in turn results in an increased parallel current that must be carried by more energetic electrons. Therefore, these results suggest that, as long as the perpendicular scale length of the wave is $\mathcal{O}(\lambda_e)$ at high latitudes, a large ratio between the torus and high-latitude densities can actually act to enhance the broadband auroral emissions at Jupiter. Additionally, since a more realistic heavy ion mass in the torus will also act to reduce the wave group speed and increase the ion kinetic energy (for a given perpendicular electric field perturbation), it is expected that a more realistic consideration of the average ion mass in the torus will only further enhance the broadband electron energization noted here. However, we will address this idea more specifically in a follow-up study.

In this work, we have neglected consideration of ion gyroradius effects for initial simplicity, but we note that earlier works (Chaston, Bonnell, Carlson, McFadden, Strangeway, & Ergun, 2003; Damiano et al., 2015, 2016), for parameters relevant to the terrestrial magnetosphere, have illustrated that the extent of the broadband energization actually decreases with increases in $\frac{T_i}{T_e}$. To first order such a result can be inferred from simple two fluid analysis where the ratio of the parallel and perpendicular electric field is inversely proportional to the ion gyroradius (e.g., Chaston, Bonnell, Carlson, McFadden, Strangeway, & Ergun, 2003; Streltsov et al., 1998)

$$E_{||}/E_{\perp} = \frac{-k_{||}k_{\perp}\rho_s^2}{(1+k_{\perp}^2\rho_i^2)}. \tag{7}$$

(where $\rho_s = (T_e/m_i)^{1/2}/\Omega_i$ is the ion acoustic length). Therefore, what we are presenting here may represent the maximum extent of the energization for the considered wave parameters. Additionally, similar behavior with increases of $\frac{T_i}{T_e}$ was noted in studies of the propagation of kinetic Alfvén waves in the Io plasma torus using the GKE model considering more realistic ion masses and temperatures than were used here. Another complexity over the terrestrial example is that the ambipolar electric fields that exist at the torus boundaries, in order to maintain quasi-neutrality, can also act to trap electrons within the torus itself.

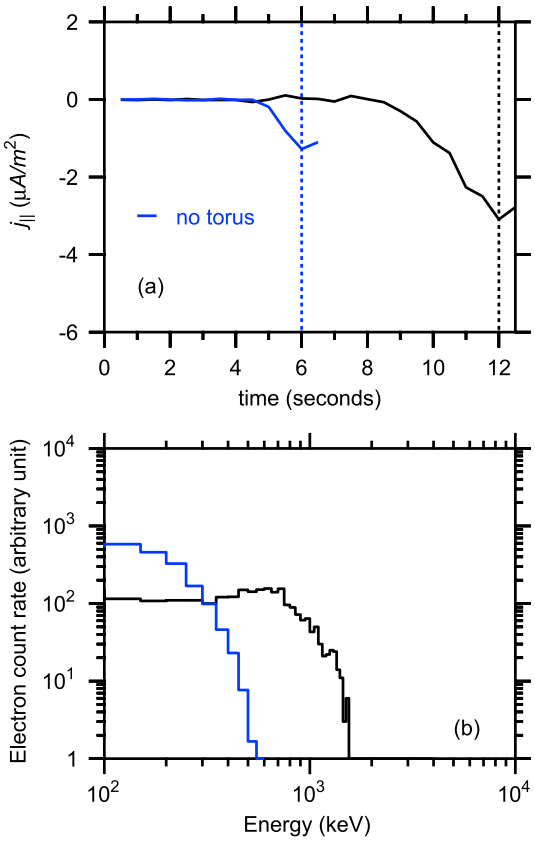

Figure 5. (a) Parallel current above the low-altitude boundary as a function of time with and without torus. (b) Corresponding histograms of electron count rate versus energy at the peak of the parallel current as indicated in Figure 5a.

Finally, it is worth emphasizing that, although we suggested that wave energy at dispersive scales can be fed by a turbulent cascade, the broadband energization evident here is the result of energization essentially in a single flux tube with a specific dominant equatorial perpendicular scale length (e.g., see Figure 1b). This choice was made in order to understand the nature of the energization in a single component of such a turbulent spectrum. However, it is important to realize that this flux tube in itself is representative of a range of perpendicular scale lengths that the wave evolves through. Using the same model approach, Damiano and Wright (2005) considered electron energization by inertial Alfvén waves in a uniform magnetic field topology and, in that instance, the parallel wave current was carried by a uniform drift of the entire distribution function that looked monoenergetic in nature. In the example presented here, because of the converging magnetic field topology, the wave evolves through a range of perpendicular scale lengths (even in the inertial Alfven wave limit), which suggests that this nonuniformity in the topology is a key factor in the resulting broadband electron energy signature. In the limit that we also initialize with an energy spectrum in the torus region (more consistent with the idea of a turbulent cascade), we expect that the qualitative characteristics of the energization will not change. This is because we are simply adding another source of perpendicular scale lengths (in addition to the topology) and the aggregate effect on the electron energization should still look broadband. A more detailed analysis of these (and the ρ_i effects discussed above) will be more completely addressed in a follow-up manuscript.

4. Conclusions

In this work, a 2-D GKE model has been used to investigate electron energization at Jupiter due to Alfvén waves sourced in the Io plasma torus. Consistent with both the recent observations at Jupiter and those seen in the terrestrial magnetosphere, the electron energization due to dispersive scale Alfvén waves is broadband in nature. For the considered parameters, the bulk of the energization is the result of the nonresonant interaction between inertial Alfvén waves and electrons at high latitudes. A characteristic unique to the

case of Jupiter is that the presence of the plasma torus can act to enhance the magnitude of the energization owing to the extra energy the increased ion density imparts to the wave for a given perturbation of the perpendicular electric field.

Acknowledgments
The authors acknowledge support from NASA grants NNH14AY11I, NNH15AZ95I, 80NSSC18K1578, and 80NSSC18K0835 and NSF grant AGS1832207. Simulation data used in the figures may be accessed at https://github.com/padamiano/GRL2019data website.

References

Allegrini, F., Bagenal, F., Bolton, S., Connerney, J., Clark, G., Ebert, R. W., et al. (2017). Electron beams and loss cones in the auroral regions of Jupiter. *Geophysical Research Letters*, *44*, 7131–7139. https://doi.org/10.1002/2017GL073180

Bonfond, B., Saur, J., Grodent, D., Badman, S. V., Bisikalo, D., Shematovich, V., et al. (2017). The tails of the satellite auroral footprints at Jupiter. *Journal of Geophysical Research: Space Physics*, *122*, 7985–7996. https://doi.org/10.1002/2017JA024370

Chaston, C. C., Bonnell, J. W., Carlson, C. W., McFadden, J. P., Ergun, R. E., & Strangeway, R. J. (2003). Properties of small-scale Alfvén waves and accelerated electrons from FAST. *Journal of Geophysical Research*, *108*(A4), 8003. https://doi.org/10.1029/2002JA009420

Chaston, C. C., Bonnell, J. W., Carlson, C. W., McFadden, J. P., Strangeway, R. J., & Ergun, R. E. (2003). Kinetic effects in the acceleration of auroral electrons in small scale Alfvén waves: A FAST case study. *Geophysical Research Letters*, *30*(6), 1289. https://doi.org/10.1029/2002GL015777

Chaston, C. C., Bonnell, J. W., Peticolas, L. M., Carlson, C. W., McFadden, J. P., & Ergun, R. E. (2002). Driven Alfvén waves and electron acceleration: A fast case study. *Geophysical Research Letters*, *29*(11), 1535. https://doi.org/10.1029/2001GL013842

Chust, T., Roux, A., Kurth, W. S., Gurnett, D. A., Kivelson, M. G., & Khurana, K. K. (2005). Are Io's Alfvén wings filamented? Galileo observations. *Planetary and Space Science*, *53*, 395–412. https://doi.org/10.1016/j.pss.2004.09.021

Cowley, S. W. H., & Bunce, E. J. (2001). Origin of the main auroral oval in Jupiter's coupled magnetosphere-ionosphere system. *Planetary and Space Science*, *49*, 1067–1088.

Crary, F. J. (1997). On the generation of an electron beam by Io. *Journal of Geophysical Research*, *102*, 37.

Damiano, P. A., Chaston, C. C., Hull, A. J., & Johnson, J. R. (2018). Electron distributions in kinetic scale field line resonances: A comparison of simulations and observations. *Geophysical Research Letters*, *45*, 5826–5835. https://doi.org/10.1029/2018GL077748

Damiano, P. A., & Johnson, J. R. (2012). Electron acceleration in a geomagnetic field line resonance. *Geophysical Research Letters*, *39*, L02102. https://doi.org/10.1029/2011GL050264

Damiano, P. A., Johnson, J. R., & Chaston, C. C. (2015). Ion temperature effects on magnetotail Alfvén wave propagation and electron energization. *Journal of Geophysical Research: Space Physics*, *120*, 5623–5632. https://doi.org/10.1002/2015JA021074

Damiano, P. A., Johnson, J. R., & Chaston, C. C. (2016). Ion gyroradius effects on particle trapping in kinetic Alfvén waves along auroral field lines. *Journal of Geophysical Research: Space Physics*, *121*, 10,831–10,844. https://doi.org/10.1002/2016JA022566

Damiano, P. A., & Wright, A. N. (2005). Two-dimensional hybrid MHD-kinetic simulations of an Alfvén wave pulse. *Journal of Geophysical Research*, *110*, A01201. https://doi.org/10.1029/2004JA010603

Damiano, P. A., & Wright, A. N. (2008). Electron thermal effects in standing shear Alfvén waves. *Journal of Geophysical Research*, *113*, A09219. https://doi.org/10.1029/2008JA013087

Damiano, P. A., Wright, A. N., Sydora, R. D., & Samson, J. C. (2005). Hybrid magentohydrodynamic-kinetic electron closure methods and shear Alfvén waves in nonuniform plasmas. *Physics, Plasmas*, *12*, 42105.

Damiano, P. A., Wright, A. N., Sydora, R. D., & Samson, J. C. (2007). Energy dissipation via electron energization in standing shear Alfvén waves. *Physics of Plasmas*, *14*(6), 62904. https://doi.org/10.1063/1.2744226

Delamere, P. A., Burkholder, B., & Ma, X. (2018). Three-dimensional hybrid simulation of viscous-like processes at Saturn's magnetopause boundary. *Geophysical Research Letters*, *45*, 7901–7908. https://doi.org/10.1029/2018GL078922

Gombosi, T. I., Tóth, G., de Zeeuw, D. L., Hansen, K. C., Kabin, K., & Powell, K. G. (2002). Semirelativistic magnetohydrodynamics and physics-based convergence acceleration. *Journal of Computational Physics*, *177*, 176–205. https://doi.org/10.1006/jcph.2002.7009

Hess, S. L. G., Delamere, P., Dols, V., Bonfond, B., & Swift, D. (2010). Power transmission and particle acceleration along the Io flux tube. *Journal of Geophysical Research*, *115*, A06205. https://doi.org/10.1029/2009JA014928

Iroshnikov, P. S. (1963). Turbulence of a conducting fluid in a strong magnetic field. *Astronomicheskii Zhurnal*, *40*, 742.

Johnson, J. R., & Cheng, C. Z. (2001). Stochastic ion heating at the magnetopause due to kinetic Alfvén waves. *Geophysical Research Letters*, *28*, 4421–4424. https://doi.org/10.1029/2001GL013509

Keiling, A., Wygant, J. R., Cattell, C. A., Mozer, F. S., & Russell, C. T. (2003). The global morphology of wave Poynting flux: Powering the aurora. *Science*, *299*, 383–386. https://doi.org/10.1126/science.1080073

Kletzing, C. A. (1994). Electron acceleration by kinetic Alfvén waves. *Journal of Geophysical Research*, *99*, 11,095–11,104. https://doi.org/10.1029/94JA00345

Kraichnan, R. H. (1965). Inertial-range spectrum of hydromagnetic turbulence. *Physics of Fluids*, *8*, 1385–1387. https://doi.org/10.1063/1.1761412

Lysak, R., & Lotko, W. (1996). On the kinetic dispersion relation for shear Alfvén waves. *Journal of Geophysical Research*, *101*, 5085.

Mauk, B. H., Haggerty, D. K., Jaskulek, S. E., Schlemm, C. E., Brown, L. E., Cooper, S. A., et al. (2017). The Jupiter Energetic Particle Detector Instrument (JEDI) investigation for the Juno Mission. *Space Science Reviews*, *213*, 289–346. https://doi.org/10.1007/s11214-013-0025-3

Mauk, B. H., Haggerty, D. K., Paranicas, C., Clark, G., Kollmann, P., Rymer, A. M., et al. (2017a). Discrete and broadband electron acceleration in Jupiter's powerful aurora. *Nature*, *549*, 66–69. https://doi.org/10.1038/nature23648

Mauk, B. H., Haggerty, D. K., Paranicas, C., Clark, G., Kollmann, P., Rymer, A. M., et al. (2017b). Juno observations of energetic charged particles over Jupiter's polar regions: Analysis of monodirectional and bidirectional electron beams. *Geophysical Research Letters*, *44*, 4410–4418. https://doi.org/10.1002/2016GL072286

McComas, D. J., Alexander, N., Allegrini, F., Bagenal, F., Beebe, C., Clark, G., et al. (2017). The Jovian Auroral Distributions Experiment (JADE) on the Juno mission to Jupiter. *Space Science Reviews*, *213*, 547–643. https://doi.org/10.1007/s11214-013-9990-9

Ng, C. S., & Bhattacharjee, A. (1996). Interaction of shear-Alfven wave packets: Implication for weak magnetohydrodynamic turbulence in astrophysical plasmas. *Astrophysical Journal*, *465*, 845. https://doi.org/10.1086/177468

Ng, C. S., Delamere, P. A., Kaminker, V., & Damiano, P. A. (2018). Radial transport and plasma heating in Jupiter's magnetodisc. *Journal of Geophysical Research: Space Physics*, *123*, 661–6620. https://doi.org/10.1029/2018JA025345

Ray, L. C., Ergun, R. E., Delamere, P. A., & Bagenal, F. (2010). Magnetosphere-ionosphere coupling at Jupiter: Effect of field-aligned potentials on angular momentum transport. *Journal of Geophysical Research*, *115*, A09211. https://doi.org/10.1029/2010JA015423

Saur, J. (2004). Turbulent heating of Jupiter's middle magnetosphere. *Astrophysical Journal Letters*, *602*, L137—L140. https://doi.org/10.1086/382588

Saur, J., Janser, S., Schreiner, A., Clark, G., Mauk, B. H., Kollmann, P., et al. (2018). Wave-particle interaction of Alfvén waves in Jupiter's magnetosphere: Auroral and magnetospheric particle acceleration. *Journal of Geophysical Research: Space Physics*, *123*, 9560–9573. https://doi.org/10.1029/2018JA025948

Saur, J., Politano, H., Pouquet, A., & Matthaeus, W. H. (2002). Evidence for weak MHD turbulence in the middle magnetosphere of Jupiter. *Astronomy and Astrophysics*, *386*, 699–708. https://doi.org/10.1051/0004-6361:20020305

Stauffer, B. H. (2018). The generation of dispersive waves in the giant magnetospheres through mass loading and transport (PhD thesis), University of Alaska Fairbanks.

Streltsov, A. V., Lotko, W., Johnson, J. R., & Cheng, C. Z. (1998). Small-scale, dispersive field line resonances in the hot magnetospheric plasma. *Journal of Geophysical Research*, *103*, 26,559–26,572. https://doi.org/10.1029/98JA02679

Su, Y.-J., Jones, S. T., Ergun, R. E., Bagenal, F., Parker, S. E., Delamere, P. A., & Lysak, R. L. (2006). Io-Jupiter interaction: Alfvén wave propagation and ionospheric Alfvén resonator. *Journal of Geophysical Research*, *111*, A06211. https://doi.org/10.1029/2005JA011252

Szalay, J. R., Bonfond, B., Allegrini, F., Bagenal, F., Bolton, S., Clark, G., et al. (2018). In situ observations connected to the Io footprint tail aurora. *Journal of Geophysical Research: Planets*, *123*, 3061–3077. https://doi.org/10.1029/2018JE005752

Thorne, R. M., Armstrong, T. P., Stone, S., Williams, D. J., McEntire, R. W., Bolton, S. J., et al. (1997). Galileo evidence for rapid interchange transport in the Io torus. *Geophysical Research Letters*, *24*, 2131.

Wing, S., Gkioulidou, M., Johnson, J. R., Newell, P. T., & Wang, C.-P. (2013). Auroral particle precipitation characterized by the substorm cycle. *Journal of Geophysical Research: Space Physics*, *118*, 1022–1039. https://doi.org/10.1002/jgra.50160

Wright, A. N., Allan, W., Ruderman, M. S., & Elphic, R. C. (2002). The dynamics of current carriers in standing Alfvén waves: Parallel electric fields in the auroral acceleration region. *Journal of Geophysical Research*, *107*, 1120.